OPEN

Submerged Liquid Plasma for the Synchronized Reduction and Functionalization of Graphene Oxide

Jaganathan Senthilnathan, Yung-Fang Liu, Kodepelly Sanjeeva Rao & Masahiro Yoshimura

Promotion Centre for Global Materials Research (PCGMR), Department of Material Science and Engineering, National Cheng Kung University, Tainan, Taiwan.

Formation of reduced and functionalized graphene oxide (r-FGO) at ambient temperature and pressure is demonstrated by generating liquid plasma submerged in acetonitrile and graphene oxide solution. The partial restoration of conjugation (sp^2 domain) and insertion of fluorophores such as nitrile and amine in r-FGO displays enhanced fluorescence property. Presence of nitrile and amine in r-FGO are confirmed by X-ray photoelectron spectroscopy and Fourier transforms infrared spectroscopy. Morphology and optical property of r-FGO are studied with transmission electron microscopy, scanning tunneling microscopy and Ultraviolet–visible spectroscopy measurements. The nitrile and amine present in r-FGO undergo a surface-controlled reversible redox reaction and sp^2- enriched r-FGO acts as an electrical double layer, providing additional hybrid capacitance or pseudocapacitance. r-FGO shows high cyclic stability with a specific capacitance value of 349 F/g at the scan rate of 10 mV/s. Only marginal reduction of specific capacitance ($<$10% reduction) is observed at the end of 1000 cycles.

Carbon-based electrochemical capacitors have received considerable attention due to their extended cycle life, low maintenance, high power capability, and reliability[1,2]. Graphene has attracted great interest for applications in supercapacitor electrodes due to its remarkable optical transparency, mechanical flexibility, and electrical and thermal conductivity[2–5]. The superior properties of graphene are associated with its single layer, which is difficult to produce on a large scale due to its irreversible agglomeration at ambient conditions[6]. The strong van der Waals force of attraction between layer leads to poor dispersibility in both hydrophilic and hydrophobic solvents[7]. The functionalization of graphene is an important route for improving its dispersibility in solvent[8]. Graphene oxide (GO) is the only promising functionalized material with high dispersibility in most solvents that can be synthesized in large quantities from inexpensive graphite powder[9]. However, GO has poor electrical properties due to the presence of oxygen functional groups and a discontinuous sp^2 network[10]. To overcome the poor electrical properties, GO can be reduced and the reduced GO (r-GO) displays significant specific capacitance due to the increase in the π-π (sp^2) network when compared to GO. Furthermore, residual oxygen present in r-GO shows considerable dispersibility in solvents[11]. GO modified with conductive polymers or metal oxides have high capacitance compared to that of pristine graphene/r-GO[12]. The active group present in r-GO/graphene composite follows reversible redox as well as electrical double layer (EDL) mechanisms; such composites are called faradaic supercapacitors or pseudocapacitors[5,13]. Organic polymers such as carboxyl-functionalized GO-polyaniline and 3,4-propylenedioxythiophene/GO nanosheets have high specific capacitance[14]. However, disadvantages of organic polymers/carbon-based supercapacitor electrodes are low electrical conductance and poor cycling stability, limiting their practical application[15]. Eco-friendly and low-temperature synthesis of functionalized graphene still remains a challenge[16]. r-GO prepared by adding reducing agents are toxic and unsuitable for large-scale production[16]. Furthermore, the reduction and functionalization of GO requires a series of steps, including dispersion, filtration, washing, and drying, which increase operation cost[17].

In contrary to the various techniques reported in the literature for the formation of r-GO or functionalized GO, gas plasma or glow discharge plasma is considered an effective, economical, and eco-friendly process[16,18–21]. The major shortcomings of gas phase or glow discharge plasma with various gaseous precursors (e.g., H_2, NH_3, and N_2) are (a) high operation cost, (b) direct ion bombardment increasing disorder and damaging the surface, (c) low contact time reducing the reduction and functionalization, (d) material loss and (e) uncertainty and inconsistency of the end products[22–25]. We believe that a sustainable method for the synthesis of r-GO or functionalized GO to achieve high electrical properties and reasonable dispersibility should be a simple, efficient, eco-friendly,
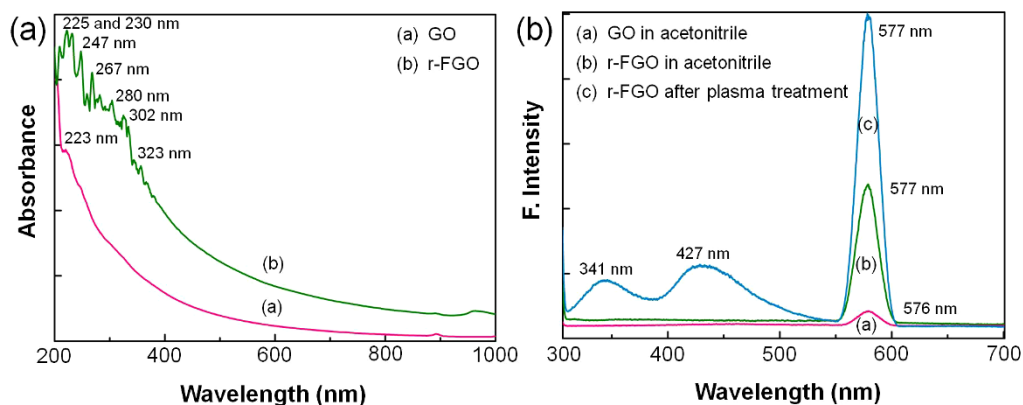
Figure 1 | (a) UV-Vis spectra of GO and r-FGO. (b) Fluorescence spectra of the GO and f-FGO in acetonitrile solution.

economical, and one-step approach. In present study, we are proposing a unique process "submerged liquid plasma (SLP)" for the synchronized reduction and functionalization of GO in acetonitrile solution at ambient condition. The influence of functional groups on the capacitive behavior of reduced and functionalized GO (r-FGO) is demonstrated.

Results

The UV-Vis absorption spectrum of GO shows a (π—π*) plasmon peak near 223 nm, which is attributed to the conjugative effect of nanometer-scale sp[2] clusters and linking chromophore, such as —C=O and —C–O groups[6,8,26]. The strong electron donation and withdrawing (through resonance and inductive effects) nature of —NH$_2$ and —C≡N groups in r-FGO increases the red shift, with UV-Vis absorptions in the range of 225–323 nm (225, 230, 247, 267, 280, 302, and 323 nm)[27,28]. The increase in absorption peaks at 225, 230 and 247 nm is attributed to the functionalization of —C≡N, —NH$_2$, and —CH=CH$_2$ groups, respectively, in the r-FGO network[27,28]. The absorption bands at 267 and 280 nm indicate an increase in the (π—π*) electronic conjugation within r-FGO[8,29]. The absorption bands at 310 and 323 nm are attributed to n—π* transitions of C=O and the coupling and cross coupling of functional groups in r-FGO, respectively[27]. UV-Vis absorption spectra for GO and r-FGO are given in Fig. 1a. Fluorescence spectra of GO composites were recorded before and after plasma treatment (Fig. 1b). Before plasma treatment, GO (dispersed in acetonitrile solvent) showed a weak fluorescence peak at 576 nm. Whereas, r-FGO showed a strong fluorescence peak at 577 nm due to the presence of fluorophores such as –C≡N, –N=O, and =C=O which increases the π-π* electronic conjugation within the reduced graphene sheet[22,30,31]. Furthermore, r-FGO showed two additional peaks

at 341 and 427 nm, which might be due to the dimerization of acetonitrile ($C_4H_4N_2$, pyrazine) radical monomers[22]. These two additional peaks disappeared when the final r-FGO solution was centrifuged and re-suspended in acetonitrile solvent. The fluorescence spectra of r-FGO are given in Fig. 1b.

The FT-IR spectra of GO and r-FGO composite are given in Fig. 2a. The FT-IR spectrum of GO shows a strong absorption band at 1645 cm^{-1}, which is attributed to the C=O and C=C stretching vibrations. The band at 3085 cm^{-1} is assigned to aromatic C–H stretching vibration. Bands corresponding to carboxy C=O, alkoxy C–O–C and epoxy C–O appear at 1635, 1321, and 952 cm^{-1}, respectively[8,22]. The stretching mode of the O–H band appears at 3382 cm^{-1} [32]. The FT-IR absorption patterns of GO significantly changed after exposure to SLP. As shown in Fig. 2a, r-FGO shows four major peaks, at 1022, 2130, 2767, and 3421 cm^{-1}. The peak at 1022 cm^{-1} is attributed to the stretching vibrations of C–O–C and in-plane bending of C—H. Bands corresponding to —C≡N, C–H (alkane C–H stretching vibrations), and N–H appeared at 2130, 2767, and 3421 cm^{-1} respectively[22,33]. The intense bands at 2130 and 3421 cm^{-1} confirm that nitrile and amine groups were successfully grafted onto the r-FGO layer. The coexistence of nitrile and amine (hydrophilic) groups and the enriched sp[2] domain (hydrophobic) in r-FGO leads to significant dispersibility in polar as well as non-polar solvents (Fig. S3).

Microstructure and chemical composition of r-FGO. The Raman spectra of GO and r-FGO show the D band (sp[3]) at 1350 and 1344 cm^{-1} and the G band (sp[2]) at 1604 and 1601 cm^{-1} (Fig. 2b). The D band corresponds to the defect-induced breathing mode of A1g symmetry and the G band corresponds to the first-order scattering of the E2g mode[18,19]. The I_D/I_G ratio and the full width
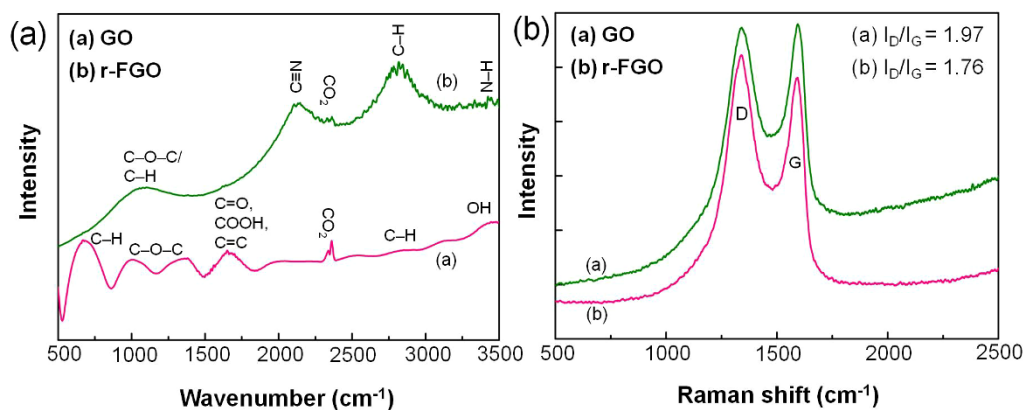
Figure 2 | (a) FTIR spectra of GO and r-FGO (b) Raman spectra of GO and r-FGO.

at half maximum (FWHM) values of the D and G bands provide information about the graphitized structure and defect/disordered structure of GO and r-FGO[34]. The FWHM values of the D and G bands for GO were 223 and 126 cm^{-1}, respectively, and those for r-FGO were 188 and 132 cm^{-1}, respectively. The I_D/I_G ratios of GO and r-FGO were 1.97 and 1.76, respectively. The decrease in the I_D/I_G ratio and D band FWHM value indicates a reduction of structural imperfections and restoration of the sp^2 domain at the r-FGO surface. The reduction of GO with glow discharge or gas plasma damages the existing graphitized structure by direct ion bombardment, resulting in greater disorder on the reduced GO surface[16,18,19]. In contrast, for the SLP process, the reduction and functionalization takes place simultaneously and without damaging the existing sp^2 domain.
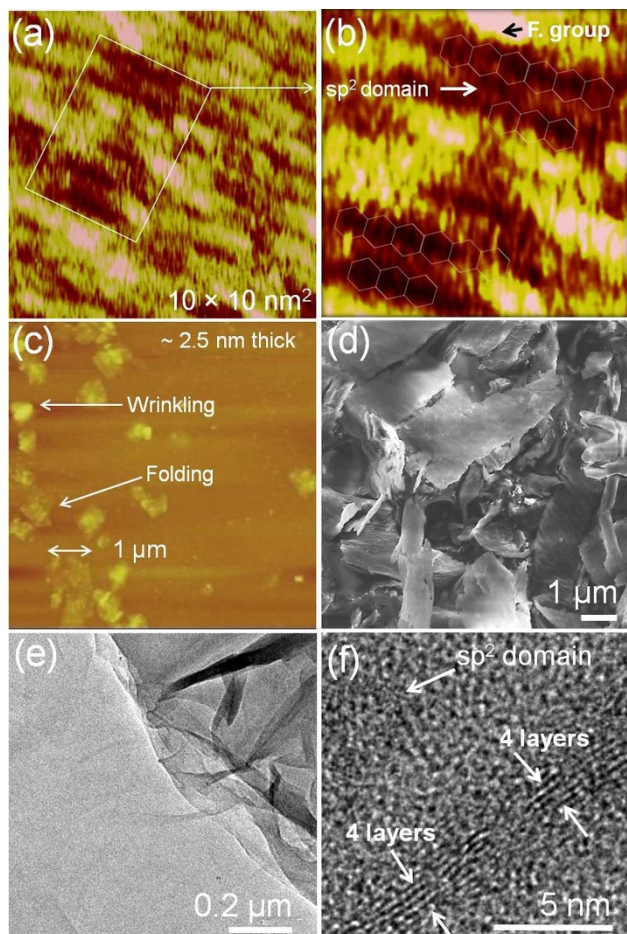
STM, HRTEM and SEM analysis were carried out to understand the atomic structure of sp^2 clusters and nanoscale morphology of r-FGO. An atomically well resolved STM image could not be obtained for GO due to the presence of sp^3 carbon (sp^3 carbon 24.8%, as determined from XPS analysis), which is surrounded by oxygen functional groups. r-FGO shows discontinuous sp^2 (sp^2 carbon 56.4%, as determined from XPS analysis) carbon domains, which can be clearly observed in STM images (Fig. 3a and Fig. 3b)[32]. Fig. 3b shows many bright regions, which correspond to —C≡N, —NH$_2$, and —CH=CH$_2$ groups, distorting the hexagonally ordered arrangement[35]. The functionalized regions (indicated by arrows) are shown in Fig. 3a and magnified in Fig. 3b. Furthermore, AFM analysis of r-FGO shows a thin layer along with folded and wrinkled layers (Fig. 3c). The formation of such layers might be due to the presence of functional groups, which are likely present at the edges of r-FGO. The thickness of the sheets varied with location. The average thickness was ∼2.5 to 5 nm (Fig. S4). SEM image of r-FGO is given in Fig. 3d. The existence of discontinuous sp^2 domains was confirmed by HRTEM analysis. GO does not show any nanoscale sp^2 domains in HRTEM analysis (Fig. S5). In contrast, r-FGO shows ∼4 layers with discontinuous sp^2 domains (Fig. 3e and f).

XPS measurements were carried out to investigate the reduction of oxygen and the level of nitrogen introduced into GO before and after plasma treatment. The XPS spectra of GO and r-FGO show the presence of carbon, nitrogen, and oxygen (Fig. 4a). The XPS spectrum of r-FGO shows that the peak intensity of O 1s is remarkably reduced and that 3.1% N is inserted after SLP treatment. Furthermore, the C/O ratios of GO (C/O = 2.3) and r-FGO (C/O = 4.64) indicate a considerable reduction of oxygen clouds and the restoration of the sp^2 carbon domain. The electronic 1s core levels of N and C were analyzed and numerically fitted with Gaussian functions for GO and r-FGO. The C 1s region of GO (Fig. 4b) consists of six well resolved binding energy configurations, identified as 284.4, 285.1, 286.3 286.9, 287.8, and 289 eV for sp^2, sp^3, C—O (epoxy/hydroxyl), C=O (carbonyl), and O—C=O (carboxyl) groups, respectively[19,31,36,37]. Similarly, the C 1s region of r-FGO (Fig. 4c) has four well resolved binding energy configurations, namely 284.8, 285.5, 287.1, and 288.3 eV for C—C, C–N, C=O, and O—C=O, respectively[36,37]. The C 1s region of r-FGO shows an intense peak at 284.8 eV (sp^2) due to the effective reduction of hydroxyl and epoxy groups and only the marginal reduction is observed for carbonyl (287.1 eV: —C=O) and carboxyl (288.3 eV: O—C=O) groups[38]. The peak corresponding to sp^2 carbon at 284.8 eV is the major feature of the C1s region. The new peak at 285.5 eV (sp^3 carbon) is attributed to the C—N bond formed by the incorporation of nitrile and amine groups into the r-FGO network. The intensity of the sp^3 carbon peak found in GO at 285.1 eV is considerably reduced and shifted to 285.5 eV after SLP treatment. Similarly, the N 1s region of r-FGO (Fig. 4d) has a broad peak at 399 eV, which can be attributed to the —C=N or —C≡N bond, and a peak at 400.1 eV, which is assigned to NH—C=O[22,38,39]. The binding energy of 401.4 eV corresponds to —NH$_2$ or quaternary NH$_3^+$ [16,22]. The above observation clearly supports the one-step simultaneous reduction and functionalization of GO in the SLP process.

Discussion

Radical-induced reduction and functionalization of GO in SLP. In the SLP process, groups like C—C (bond energy 348 kJ/mol), C—H (413 kJ/mol), C—O (360 kJ/mol), and O—H (366 kJ/mol) present in organic solvents such as methanol, ethanol, and other saturated aliphatic organic compounds form less stable radical species and favor the carbonization reaction[22–24]. The compounds containing either unsaturated or high-energy functional groups (e.g., C=C, C=N, and C≡N) form stable free radical species by the hyperconjugation effect. In the SLP process, acetonitrile first initiates hydrogen detachment and then forms the highly reactive free radical species[22]. The high-bond-energy C≡N (891 kJ/mol) group present in the acetonitrile resists the carbonization and forms stable ·H and ·CH$_2$—C≡N radicals by attacking the C—H group (Fig. 5). GO dispersed in acetonitrile solution enriched with sp^3 carbon (oxygenated carbon) contains epoxy, hydroxyl, carbonyl, and carboxyl functional groups[25]. The bulky carbonyl or carboxylic groups are preferentially attached at the edges and epoxy and hydroxyl groups lie above and below the GO sheet[25]. Very reactive nascent ·H effectively reduces epoxy and hydroxyl groups present in GO and restores the sp^2 network. Similarly, the ·CH$_2$—C≡N radical reacts with carbonyl and carboxy groups and forms amine and nitrile functional groups. A schematic representation of a possible reduction reaction with plasma under submerged conditions is given in Fig. 5. The possible radical reactions under SLP conditions with oxide functional groups are as follows.

Figure 3 | (a, b) STM image of r-FGO, (c) AFM image of r-FGO, (d) SEM image of r-FGO, and (e, f) HRTEM image of r-FGO.
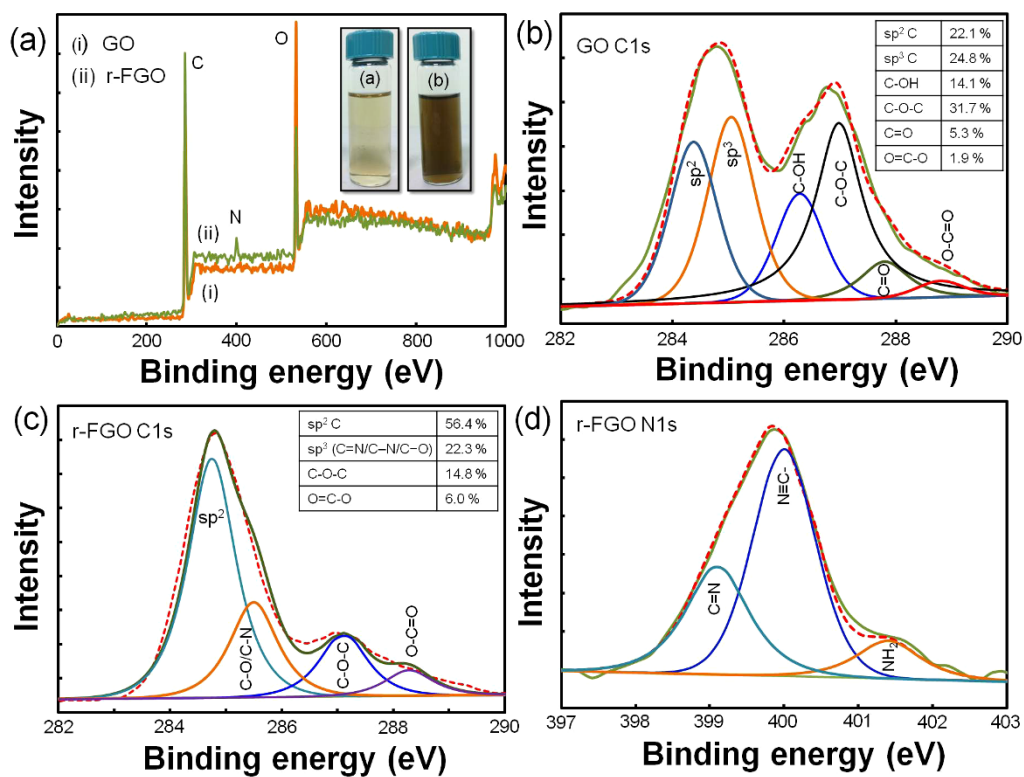
Figure 4 | (a) XPS spectra of GO and r-FGO in C 1s, N 1s, and O 1s region (b) XPS spectra of GO in C 1s region, (c) r-FGO in C 1s region, (d) r-FGO in N 1s region.
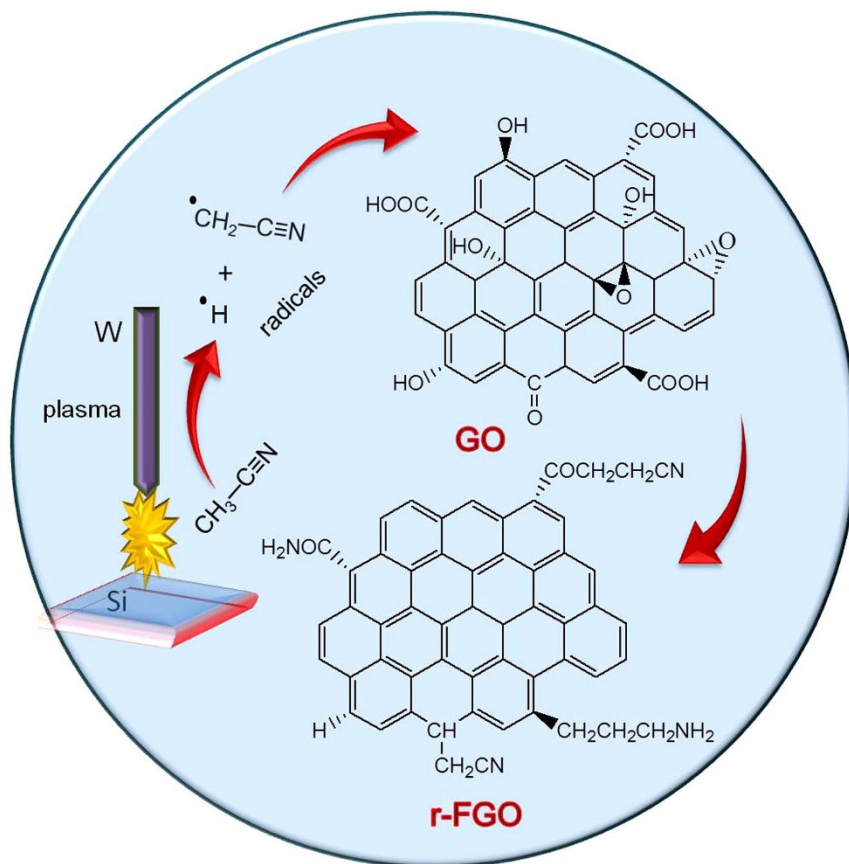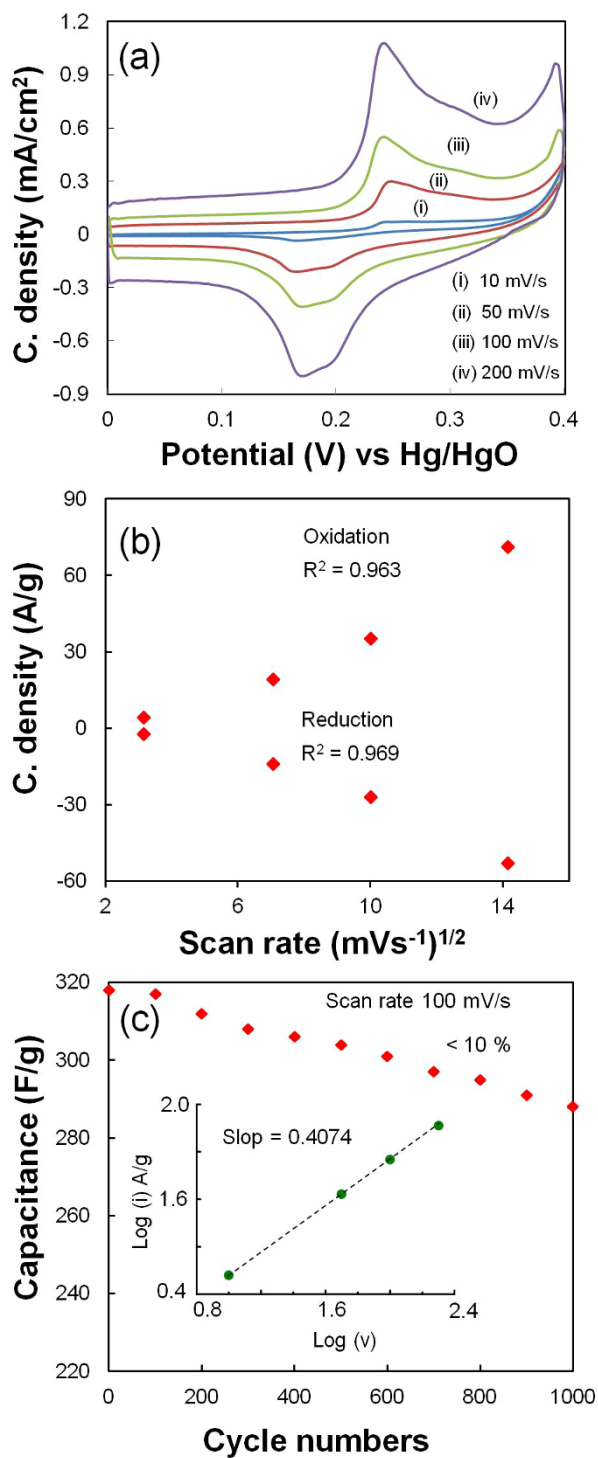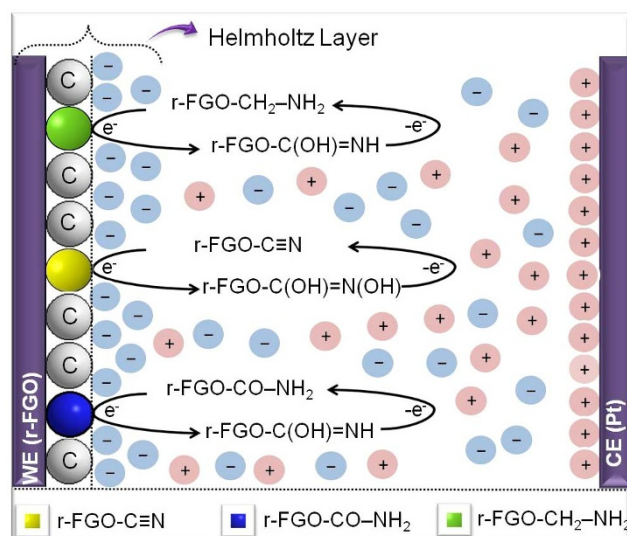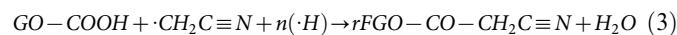

Figure 5 | Proposed mechanism of simultaneous reduction and functionalization of GO.

Figure 7 | Proposed pseudocapacitance mechanisms of functional groups present in r-FGO.

$$GO-C=O+\cdot CH_2C\equiv N+n(\cdot H)\rightarrow rFGC-O-CH=CH-NH_2 \quad (4)$$

The electrochemical properties of r-FGO were evaluated in a three-electrode system. The potential was scanned in a potential range of 0 to 0.4 V. The CV scan rate was varied from 10 to 200 mV/s. Fig. 6a shows the CV curves of r-FGO between 0 and 0.4 V obtained at scan rates of 10, 50, 100, and 200 mV/s. Each cyclic voltammogram shows a pair of well-developed redox peaks, which clearly indicates the contribution of nitrile and amine groups in the oxidation and reduction reaction[40,41]. Similar distinct oxidation reduction peaks (faradic) have been reported for the graphene oxide–polyaniline and graphene oxide-conjugated polymer (poly-3,4-propylenedioxythiophene) composites, whose specific capacitances are 525 and 201 F/g, respectively[12,14]. A comparison of the specific capacitance value of r-FGO with those in recently reported works are given in Supplementary Section Table S1. The difference between the potentials of anodic (E_{pa}) and cathodic (E_{pc}) peak-current was found to be $\Delta E_p = 61.9$ mV for the scan rates of 10 and 50 mV/s. This value indicates a well ordered reversible redox reaction and no change in the electron transfer rate[42]. Slight increases in ΔE_p values to 63.3 and 65.6 mV were observed for scan rates of 100 and 200 mV/s, respectively. These increases indicate a slight decrease in the electron transfer rates for higher scan rates (100 and 200 mV/s). The anodic and cathodic peak currents of r-FGO at various scan rates show a linear relationship with the square root of the scan rate (Fig. 6b) and are in good agreement with the Randles-Sevcik equation[43]. Furthermore, the plot of log "i" versus log "V" with a slope of 0.4 (Fig. 6c inset) clearly shows that the electron transfer is predominantly controlled by a diffusion mechanism (Fig. 7). The nitrile and amine present in r-FGO undergo a surface-controlled reversible redox reaction and the sp²-enriched r-FGO acts as an EDL, providing additional hybrid capacitance or pseudocapacitance[11]. Hence r-FGO displays an enhanced specific capacitance (349 F/g). However, the role of EDL is minimal and the redox reaction plays the major role in controlling the reaction. The specific capacitance values of r-FGO are 349, 335, 318, and 309 F/g for scan rates of 10, 50, 100, and 200 mV/s, respectively. The marginal decrease in specific capacitance value indicates a high degree of sustainability even at a high scan rate. Fig. 6c shows the cyclic stability of r-FGO at a 100 mV/s scan rate; high stability and a high degree of reversibility can be seen. Only a 10% reduction of the specific capacitance was observed at the end of 1000 cycles.

Figure 6 | (a) Electrochemical CV curves of r-FGO in 6 M KOH obtained at a scan rate of 10 to 200 mV/s. **(b)** Peak current dependence on the square root of scan rate **(c)** Cycle stability of the composite at a scan rate of 100 mV/s. Inset shows log of scan rate (log V) versus peak current (log I). Note: C. density = Current density.

$$GO-C-OH+n(\cdot H)\rightarrow rFGO-C=C+H_2O \quad (1)$$

$$GO-epoxide+n(\cdot H)\rightarrow rFGO-C=C-+H_2O \quad (2)$$

$$GO-COOH+\cdot CH_2C\equiv N+n(\cdot H)\rightarrow rFGO-CO-CH_2C\equiv N+H_2O \quad (3)$$

In conclusion, synthesis of r-FGO using nascent ˙H and ˙CH₂CN radicals with the SLP process was demonstrated. The SLP approach provides a number of advantages over the glow discharge/gas plasma process, including (a) fast moving electrons generated at the interface that are effectively quenched by acetonitrile solution, (b) minimal surface damage, (c) possibility of large-scale production, and (d) low operating cost and eco-friendliness. The nitrile- and amine-embedded r-FGO has high capacitance and cyclic stability. r-FGO synthesized by the SLP process is an attractive material for applications such as energy storage, sensors, and solar cells.

Experimental

Plasma experimental procedure and chemical used. In the plasma experiments, an etched tungsten needle was used as a point high-voltage electrode and a Si wafer was used as a planar ground electrode. All the experiments were conducted using a tungsten needle with a diameter of 50—100 μm (Fig. S1). Acetonitrile (99.95%) and GO, purchased from Sigma Aldrich, were used as the target materials. The target solution was prepared with 7.5 mL (1 mL of solution contains 0.25 mg of GO) of GO dispersed in 60 mL of acetonitrile (31 mg/L of GO in acetonitrile solution). The electrodes were immersed into the acetonitrile solution and separated by a distance of ~75 μm[22]. The electrode distance was controlled by a moving stage assembly (Translation Stage Triple-Divide Series 9064 and 9065) operated by a computer. A discharge voltage of 2.7 kV was applied (repetition rate: 10 kHz, pulse delay: 500 μs, and pulse width: 5 ms) across the electrodes using a pulse generator (AVTECH, AV-1022-C) connected to a high-voltage amplifier (TREK Model 609E-6), which can generate 0.1 to 5 kV (Fig. S2). Submerged plasma reaction in acetonitrile was carried out for a fixed reaction time of 2 h. The images of the initial and final solutions are given in Fig. S2. Final r-FGO solution was centrifuged (6000 rpm) and the residue was washed with acetonitrile to remove the dimer or polymerized acetonitrile impurity[22]. The dry weight of the r-FGO was found to be 2.1 mg. It was re-suspended in acetonitrile solvent (same as initial volume, 60 mL) and used for the absorption and fluorescence measurements.

Characterizations. Absorption spectra of GO and r-FGO were collected using an ultraviolet-visible (UV-Vis) spectrometer (SCINCO S-3100). The surface morphology of GO and r-FGO was examined using a high-resolution thermal-field-emission scanning electron microscope (FE-SEM, JEOL, JSM-7001). A high-resolution transmission electron microscope (HR-TEM, JEOL JEM 2100F) operated at 200 kV was used to observe the microstructure and surface morphology of r-FGO. The fluorescence spectra of GO and r-FGO were recorded with a fluorescence spectrophotometer (Hitachi F-4500). Raman spectroscopy analysis was performed using a confocal micro-Raman spectrometer (Renishaw inVia) with a 633-nm argon laser as the excitation source. Fourier transform-infrared (FT-IR) spectra of GO and r-FGO were recorded using the KBr disk method with a Nicolet Nexus 470. FT-IR and 30 scan was recorded for each sample with a 4 cm⁻¹ spectrum resolution. High-resolution X-ray photoelectron spectroscopy (HRXPS, PHI Quantera SXM, ULVAC Inc., Kanagawa, Japan) was employed to analyze the binding energies of carbon, nitrogen, and oxygen present in GO and r-FGO. The scanning tunneling microscopy (STM) was used for r-FGO measurements in atmosphere environment, and operated in the constant-current mode (Veeco Instruments, Inc.) throughout this study. The tip was made by cutting a Pt/Ir wire (80/20, diameter 0.25 mm). Thickness of r-FGO was measured by an atomic force microscope (AFM) (SPA-300HV, Seiko Nano Technology Inc.).

Electrochemical measurements. The supercapacitance of the r-FGO electrode was evaluated with cyclic voltammetry (CV) in 6 M KOH solution at room temperature (Auto lab PGSTAT302 potentiostat). The experiments were carried out with a conventional three-electrode system. The working electrode was prepared using a 9 : 1 weight ratio of r-FGO (0.45 mL of the dispersed r-FGO acetonitrile solution contains 15.7 μg of r-FGO) and polytetrafluoroethylene (PTFE; 0.05 mL) coated on fluorine-doped tin oxide (FTO) conducting glass. A platinum electrode was used as the counter electrode and a saturated calomel electrode (SCE) was used as the reference electrode. The potential was scanned in a potential range of 0 to 0.4 V. The CV scan rate was varied from 10 to 200 mV/s. In the three-electrode system, the average specific capacitance was calculated as $Cs = \dfrac{qa + qb}{2m\Delta V}$, where q_a and q_b are the anodic and cathodic peak current, respectively, m is the weight of the active material, and ΔV is the voltage. The area of the working electrode and mass of the coated r-FGO were ~1 cm² and ~15 μg, respectively.

1. Geim, A. K. & Novoselov, K. S. The rise of graphene. *Nat. Mater.* **6**, 183–191 (2007).
2. Simon, P. & Gogotsi, Y. Materials for electrochemical capacitors. *Nat. Mater.* **7**, 845–854 (2008).
3. Guo, F., Mukhopadhyay, A., Sheldon, B. W. & Hurt, R. H. Vertically aligned graphene layer arrays from chromonic liquid crystal precursors. *Adv. Mater.* **23**, 508–513 (2011).
4. Xu, Y. *et al.* Flexible solid-state supercapacitors based on three-dimensional graphene hydrogel films. *ACS Nano* **7**, 4042–4049 (2013).
5. Zhang, Y. *et al.* Vapor trapping growth of single-crystalline graphene flowers: Synthesis, morphology, and electronic properties. *Nano Lett.* **12**, 2810–2816 (2012).
6. Li, D., Müller, M. B., Gilje, S., Kaner, R. B. & Wallace, G. G. Processable aqueous dispersions of graphene nanosheets. *Nat. Nanotech.* **3**, 101–105 (2008).
7. Wang, G., Zhang, L. & Zhang, J. A review of electrode materials for electrochemical supercapacitors. *Chem. Soc. Rev.* **41**, 797–828 (2012).
8. Woltornist, S. J., Oyer, A. J., Carrillo, J.-M. Y., Dobrynin, A. V. & Adamson, D. H. Conductive thin films of pristine graphene by solvent interface trapping. *ACS Nano* **7**, 7062–7066 (2013).
9. Eda, G., Fanchini, G. & Chhowalla, M. Large-area ultrathin films of reduced graphene oxide as a transparent and flexible electronic material. *Nat. Nanotechnol.* **3**, 270–274 (2008).
10. Eda, G. & Chhowalla, M. Chemically derived graphene oxide: Towards large-area thin-film electronics and optoelectronics. *Adv. Mater.* **22**, 2392–2415 (2010).
11. Kuila, T., Mishra, A. K., Khanra, P., Kimc, N. H. & Lee, J. H. Recent advances in the efficient reduction of graphene oxide and its application as energy storage electrode materials. *Nanoscale* **5**, 52–71 (2013).
12. Liu, Y., Deng, R., Wang, Z. & Liu, H. Carboxyl-functionalized graphene oxide–polyaniline composite as a promising supercapacitor material. *J. Mater. Chem.* **22**, 13619–13624 (2012).
13. Anjos, D. M. *et al.* Pseudocapacitance and performance stability of quinone-coated carbon onions. *Nano Energy* **2**, 702–712 (2013).
14. Kumar, N. A., Choi, H. J., Bund, A., Baek, J. B. & Jeong, Y. T. Electrochemical supercapacitors based on a novel graphene/conjugated polymer composite system. *J. Mater. Chem.* **22**, 12268–12274 (2012).
15. Liang, Y. *et al.* An advanced carbonaceous porous network for high-performance organic electrolyte supercapacitors. *J. Mater. Chem. A* **1**, 7000–7005 (2013).
16. Kim, M. J. *et al.* Fast and low-temperature reduction of graphene oxide films using ammonia plasma. *AIP Adv.* **3**, 012117 (2013).
17. Liu, Z., Duan, X., Qian, G., Zhou, X. & Yuan, W. Ecofriendly one pot synthesis of highly dispersible functionalized graphene nanosheets with free amino groups. *Nanotech.* **24**, 045609 (2013).
18. Lee, S. W., Mattevi, C., Chhowalla, M. & Sankaran, R. M. Plasma-assisted reduction of graphene oxide at low temperature and atmospheric pressure for flexible conductor applications. *J. Phys. Chem. Lett.* **3**, 772–777 (2012).
19. Kumar, N. A. *et al.* Plasma-assisted simultaneous reduction and nitrogen doping of graphene oxide nanosheets. *J. Mater. Chem. A* **1**, 4431–4435 (2013).
20. Yu, Y., Li, Y., Pan, Y. & Liu, C. J. Fabrication of palladium/graphene oxide composite by plasma reduction at room temperature. *Nanoscale Res. Lett.* **7**, 234–237 (2012).
21. Wang, Q., Li, J., Song, Y. & Wang, X. Facile synthesis of high-quality plasma-reduced graphene oxide with ultrahigh 4,4′-Dichlorobiphenyl adsorption capacity. *Chem. Asian J.* **8**, 225–231 (2013).
22. Senthilnathan, J., Weng, C. C., Liao, J. D. & Yoshimura, M. Submerged liquid plasma for the synthesis of unconventional nitrogen polymers. *Sci. Rep.* **3**, 2414–2419 (2013).
23. Wang, H. & Yoshimura, M. Electrodeposition of diamond like carbon films in organic solvents using thin wire anode. *Chem. Phys. Lett.* **348**, 7–10 (2001).

24. Watanabe, T., Wang, H., Yamakawa, Y. & Yoshimura, M. Direct carbon patterning on a conducting substrate in an organic liquid. *Carbon* **44**, 799–823 (2006).

25. Georgakilas, V. *et al.* Functionalization of graphene: Covalent and non-covalent approaches, derivatives and applications. *Chem. Rev.* **112**, 6156–6214 (2012).

26. Lai, Q., Zhu, S., Luo, X., Zou, M. & Huang, S. Ultraviolet-visible spectroscopy of graphene oxides. *AIP Adv.* **2**, 032146 (2012).

27. Jahan, M., Bao, Q. & Loh, K. P. Electrocatalytically active graphene-porphyrin MOF composite for oxygen reduction reaction. *J. Am. Chem. Soc.* **134**, 6707–6713 (2012).

28. Udaya Sri, N., Chaitanya, K., Prasad, M. V. S., Veeraiah, V. & Veeraiah, A. FT-IR, FT-Raman and UV–Vis spectra and DFT calculations of 3-cyano-4-methylcoumarin. *Spectrochim. Acta. Mol. Biomol. Spectros.* **97**, 728–736 (2012).

29. Rance, G. A., Marsh, D. H., Nicholas, R. J. & Khlobystov, A. N. UV–vis absorption spectroscopy of carbon nanotubes: Relationship between the π-electron plasmon and nanotube diameter. *Chem. Phys. Lett.* **493**, 19–23 (2010).

30. Shi, J. M. *et al.* Polynitrile-bridged two-dimensional crystal: Eu(III) complex with strong fluorescence emission and NLO property. *Chem. Commun.* **7**, 756–757 (2002).

31. Chien, C.-T. *et al.* Tunable photoluminescence from graphene oxide. *Angew. Chem. Int. Ed.* **51**, 6662–6666 (2012).

32. Pham, V. H. *et al.* Chemical functionalization of graphene sheets by solvothermal reduction of a graphene oxide suspension in N-methyl-2-pyrrolidone. *J. Mater. Chem.* **21**, 3371–3377 (2011).

33. Zhan, Y. *et al.* Oriented growth of magnetite along the carbon nanotubes via covalently bonded method in a simple solvothermal system. *Mater. Sci. Eng. B* **176**, 779–784 (2011).

34. Senthilnathan, J., Weng, C. C., Tsai, W.-T., Gogotsi, Y. & Yoshimura, M. Synthesis of carbon films by electrochemical etching of SiC with hydrofluoric acid in nonaqueous solvents. *Carbon* **71**, 181–189 (2014).

35. Vadukumpully, S., Gupta, J., Zhang, Y., Xu, G. Q. & Valiyaveettil, S. Functionalization of surfactant wrapped graphene nanosheets with alkylazides for enhanced dispersibility. *Nanoscale* **3**, 303–308 (2011).

36. Chen, W. F., Yan, L. F. & Bangal, P. R. Chemical reduction of graphene oxide to graphene by sulfur-containing compounds. *J. Phys. Chem. C* **114**, 19885–19890 (2010).

37. Huang, Z. D. *et al.* Self-assembled reduced graphene oxide/carbon nanotube thin films as electrodes for supercapacitors. *J. Mater. Chem.* **22**, 3591–3599 (2012).

38. Beck, A. J. *et al.* Plasma co-polymerisation of two strongly interacting monomers: acrylic acid and allylamine. *Plasma Processes Polym.* **2**, 641–649 (2005).

39. Rangan, S. *et al.* Surface reactions of 3-butenenitrile on the Si(001)-2 × 1 surface at room temperature. *J. Phys. Chem. B* **109**, 12899–12908 (2005).

40. Filik, H., Çetintaş, G., Avan, A. A., Koç, S. N. & Boz, I. Electrochemical sensing of acetaminophen on electrochemically reduced graphene oxide-nafion composite film modified electrode. *Int. J. Electrochem. Sci.* **8**, 5724–5737 (2013).

41. Senthilnathan, J., Sanjeeva Rao, K. & Yoshimura, M. Submerged liquid plasma – low energy synthesis of nitrogen-doped graphene for electrochemical applications. *J. Mater. Chem A.* **2**, 3332–3337 (2014).

42. Shankar, S. S. *et al.* Electrocatalytic oxidation of dopamine on acrylamide modified carbon paste electrode: A voltammetric study. *Int. J. Electrochem. Sci.* **5**, 944–954 (2010).

43. Shang, N. G. *et al.* Catalyst-free efficient growth, orientation and biosensing properties of multilayer graphene nanoflake films with sharp edge planes. *Adv. Funct. Mater.* **18**, 3506–3514 (2008).

Acknowledgments

Author contributions

M.Y. and J.S.N. performed the experimental planning, experimental measurements, data examination, and manuscript preparation. Y.F.L. contributed to the experimental setup, planning, and data analysis. K.S.R. contributed to the experimental setup and optimized plasma discharge in a submerged condition.

Additional information

Supplementary information accompanies this paper at http://www.nature.com/scientificreports

Competing financial interests: The authors declare no competing financial interests.

How to cite this article: Senthilnathan, J., Liu, Y.-F., Rao, K.S. & Yoshimura, M. Submerged Liquid Plasma for the Synchronized Reduction and Functionalization of Graphene Oxide. *Sci. Rep.* **4**, 4395; DOI:10.1038/srep04395 (2014).